Caspase-8 controls the secretion of inflammatory lysyl-tRNA synthetase in exosomes from cancer cells

Sang Bum Kim,[1,2] Hye Rim Kim,[1] Min Chul Park,[1] Seongmin Cho,[1,2] Peter C. Goughnour,[1,2] Daeyoung Han,[1,2] Ina Yoon,[1] YounHa Kim,[1,2] Taehee Kang,[1] Eunjoo Song,[3] Pilhan Kim,[3] Hyosun Choi,[4] Ji Young Mun,[4,5] Chihong Song,[6] Sangmin Lee,[7] Hyun Suk Jung,[7] and Sunghoon Kim[1,2]

[1]Medicinal Bioconvergence Research Center, Seoul National University, Suwon, South Korea
[2]Department of Molecular Medicine and Biopharmaceutical Sciences, Graduate School of Convergence Science and Technology, Seoul National University, Seoul, South Korea
[3]Graduate School of Nanoscience and Technology, Korea Advanced Institute of Science and Technology, Daejeon, South Korea
[4]BK21 Plus Program, Department of Senior Healthcare, Graduate School, Eulji University, Daejeon, South Korea
[5]Department of Biomedical Laboratory Science, College of Health Sciences, Eulji University, Seongnam, South Korea
[6]National Institute for Physiological Sciences, Okazaki, Japan
[7]Department of Biochemistry, College of Natural Sciences, Kangwon National University, Chuncheon, South Korea

Aminoacyl-tRNA synthetases (ARSs), enzymes that normally control protein synthesis, can be secreted and have different activities in the extracellular space, but the mechanism of their secretion is not understood. This study describes the secretion route of the ARS lysyl-tRNA synthetase (KRS) and how this process is regulated by caspase activity, which has been implicated in the unconventional secretion of other proteins. We show that KRS is secreted from colorectal carcinoma cells within the lumen of exosomes that can trigger an inflammatory response. Caspase-8 cleaved the N-terminal of KRS, thus exposing a PDZ-binding motif located in the C terminus of KRS. Syntenin bound to the exposed PDZ-binding motif of KRS and facilitated the exosomic secretion of KRS dissociated from the multi-tRNA synthetase complex. KRS-containing exosomes released by cancer cells induced macrophage migration, and their secretion of TNF-α and cleaved KRS made a significant contribution to these activities, which suggests a novel mechanism by which caspase-8 may promote inflammation.

Introduction

Aminoacyl-tRNA synthetases (ARSs) are known as essential enzymes for protein synthesis that charge amino acids to their cognate tRNAs (Ibba and Soll, 2000). However, they have also been recognized as unique signal mediators that are connected to diverse signal pathways (Guo and Schimmel, 2013). Among the various activities shown for ARSs, many involve the secretion of ARSs into the extracellular space (Son et al., 2014). Secreted ARSs have been reported to play roles in the control of angiogenesis (Mirando et al., 2014), immune responses (Park et al., 2005b; Han et al., 2007; Nechushtan et al., 2009), tissue regeneration (Park et al., 2005c), and tumorigenesis (Park et al., 2005a, 2012; Choi et al., 2011). However, their secretion pathways remain unknown. One of the secreted ARSs, lysyl-tRNA synthetase (KRS), was previously shown to be secreted from cancer cells to induce inflammatory responses (Park et al., 2005b). To gain insight into the secretion mechanism of ARSs, we first focused on the secretion of KRS and investigated the details of how it is secreted from cancer cells.

Human cytosolic KRS is comprised of 597 aa, into which the anticodon-binding (S70-P214) and catalytic domains (L220-K574) are embedded (Fig. 1 A; Guo et al., 2008). It also contains a unique N-terminal extension (Guo et al., 2010). Guided by specific phosphorylation events, human KRS undergoes structural transformation to exert distinct roles. For instance, it is phosphorylated in activated mast cells at S207 (Yannay-Cohen et al., 2009; Ofir-Birin et al., 2013) located at the junction of the two functional domains, and its phosphorylation dissociates these domains apart, inactivating its enzymatic role. The S207-phosphorylated KRS is then translocated into the nucleus for transcriptional control through microphthalmia-associated transcription factor (MITF). Additionally, KRS is phosphorylated by a laminin signal at T52 located in the N-terminal extension. This phosphorylation induces unfolding of the N-terminal extension, which is then guided to the plasma membrane. The membrane-bound KRS interacts with the 67-kD laminin receptor to promote cell migration (Kim et al., 2012) and cancer metastasis (Kim et al., 2014). In this study,

Correspondence to Sunghoon Kim: sungkim@snu.ac.kr

Abbreviations used: ARS, aminoacyl-tRNA synthetase; BFA, brefeldin A; BiFC, bimolecular fluorescence complementation; EPRS, glutamyle-prolyl-tRNA synthetase; KRS, lysyl-tRNA synthetase; MSC, multi-tRNA synthetase complex; MVB, multivesicular body.

The Rockefeller University Press
J. Cell Biol. Vol. 216 No. 7 2201–2216
https://doi.org/10.1083/jcb.201605118

we present the results of our investigation into how KRS is secreted to extracellular space and whether any posttranslational modifications are involved in this process.

Results

KRS secretion via exosomes

Because many proteins are secreted via the ER–Golgi pathway (Lacy and Stow, 2011), we investigated whether the secretion of KRS would also involve this pathway by using brefeldin A (BFA), which is an inhibitor of the ER–Golgi secretion pathway (Rosa et al., 1992). Because we had previously observed that the secretion of KRS was induced under starvation conditions in the presence of TNF-α (Park et al., 2005b), we compared the KRS secretion with and without BFA treatment and found no effect of BFA treatment on the KRS secretion (Fig. S1 A). In addition, we used the SignalP database to search for a potential signal peptide in KRS that could mediate secretion through the ER–Golgi pathway, and we did not detect a candidate sequence (not depicted); instead, KRS contains a PDZ domain–binding motif in its C-terminal end (Fig. 1 A, black box; Fabre et al., 2000), which is known to meditate an interaction with syntenin involved in exosome secretion (Meerschaert et al., 2008; Baietti et al., 2012). We thus assumed that KRS may be secreted by extracellular vesicles such as exosomes.

To investigate whether the KRS secretion involves secretory vesicles, we subjected complete and starvation culture media of HCT116 cells to centrifugation at 100,000 *g*. We then isolated the vesicles in the pellets, lysed the contained proteins, and detected KRS by immunoblotting with an anti-KRS antibody. When equivalent amounts of total protein were loaded for gel electrophoresis, we detected higher levels of KRS in vesicles isolated from the starvation medium than from the complete medium (Fig. 1 B). We then introduced different stresses and stimuli to HCT116 cells to identify a condition or conditions that could induce secretion of KRS from HCT116 cells. Among the tested conditions, which included starvation, TNF-α, reactive oxygen stress by sodium arsenite (Barchowsky et al., 1999; Ruiz-Ramos et al., 2009), hypoxia by $CoCl_2$ (Piret et al., 2002), and ER stress by tunicamycin, KRS secretion was most prominent upon starvation (Fig. S1 B). Interestingly, the molecular weight of secreted KRS appeared to be slightly smaller than that of the cytosolic KRS, suggesting a potential peptide cleavage of KRS during the secretion process. Density-gradient centrifugation analyses of the isolated vesicles showed that KRS is harbored in fractions within the density range of 1.09–1.15 g/ml, which also contained syntenin (Fig. 1 C). A dynamic light scattering system suggested that the KRS-containing vesicles were 147.3 nm in diameter (Fig. 1 D). Electron microscopic analysis showed cup-shaped vesicles (Fig. 1 E) that are morphologically similar to the typical exosomes (Théry et al., 2009). We also investigated whether KRS secretion was affected by suppression of Rab GTPases (Rab11a, Rab27a, and Rab35), which have been suggested to play a role in exosome shedding (Savina et al., 2005; Hsu et al., 2010; Ostrowski et al., 2010). The KRS secretion was differentially reduced by the suppression of Rab proteins (mostly significantly by Rab35, then Rab27a, and then weakly by Rab11a; Fig. 1 F), implying that KRS exosomes might be exported out of cells in a Rab-dependent manner. Because ESCRT-III proteins were previously suggested to induce luminal vesicle formation of multivesicular bodies (MVBs) and exosomic secretion of syntenin (Baietti et al., 2012), we also examined whether KRS secretion would be affected by the suppression of ESCRT-III proteins and observed the reduction of KRS and syntenin secretion by the suppression of each ESCRT-III component (CHMP1a, 2a, 3, 4a, 4b, 6, and 7; Fig. 1 G). These results further support the syntenin-dependent exosomal secretion pathway.

We used an immunogold-conjugated KRS antibody to determine the location of KRS in the isolated exosomes by immunogold-staining EM, and KRS was detected in the lumen of exosomes (Figs. 1 H and S2 A), whereas CD63, a known membrane marker of exosomes, was detected in the membrane (Fig. 1 I; Théry et al., 2002; Marzesco et al., 2005). We further determined the KRS topology in the isolated exosomes by trypsin treatment because proteins located within the lumen of exosomes would be protected from protease cleavage. When we subjected the isolated exosomes to trypsin digestion, KRS and syntenin were resistant, whereas CD63 was sensitive to trypsin cleavage (Fig. 1 J). When the vesicles were treated with 0.1% Triton X-100, all of the three proteins were digested by trypsin, further confirming that trypsin resistance of KRS was caused by the barrier of the exosome membrane.

The naked KRS was previously shown to activate macrophages, indicating that the exosome would not be essential for the signaling activity of KRS (Park et al., 2005b). To have an insight into how KRS in the lumen of exosomes can activate macrophages, we treated macrophages with KRS-containing exosomes and monitored the locations of KRS in the exosomes and macrophages by immunogold-staining EM. Although KRS was mainly detected in the lumen of exosomes (Figs. 1 K and S2, A and B), it was detected outside of the exosomes near macrophages (Figs. 1 L and S2 C) and within macrophages (Figs. 1 M and S2 D). In addition, we expressed C-terminally Myc-tagged KRS (KRS-Myc) in HCT116 cells and prepared exosomes harboring KRS-Myc. We then treated macrophages with these exosomes and monitored whether KRS-Myc taken up to the macrophages was sensitive to proteolytic cleavage. If KRS-Myc would be taken up to macrophages as naked protein, it would be sensitive to proteolytic cleavage. When KRS-Myc in the macrophages were subjected to immunoblotting at time intervals, we did not detect intact KRS-Myc in macrophages (Fig. S1 C). Although all of these results are supportive to the release of KRS from the vesicles for its action to target cells, further detailed investigation is needed to fully understand how KRS carried by the vesicles can be sensed by the target cells.

To determine whether KRS is specifically recruited to the starvation-induced exosomes, we examined the presence of nine different ARSs and found only KRS in the isolated exosomes (Fig. S1 D), suggesting the preferential recruitment of KRS to starvation-induced exosomes. We also tested several different cancer cell lines for the secretion of KRS exosomes and found that MCF7 cells also secreted KRS (Fig. S1 E).

Requirement of syntenin for KRS secretion

Prompted by recent work suggesting the potential interaction of KRS with syntenin (Meerschaert et al., 2008; Baietti et al., 2012), we tested whether syntenin plays a role in the secretion of KRS. First, we coimmunoprecipitated syntenin and KRS under complete, starved, and TNF-α treatment conditions. The starvation condition (with and without TNF-α) increased the interaction of the two proteins (Fig. 2 A). The cellular interaction of the two proteins was also monitored by a bimolecular fluo-

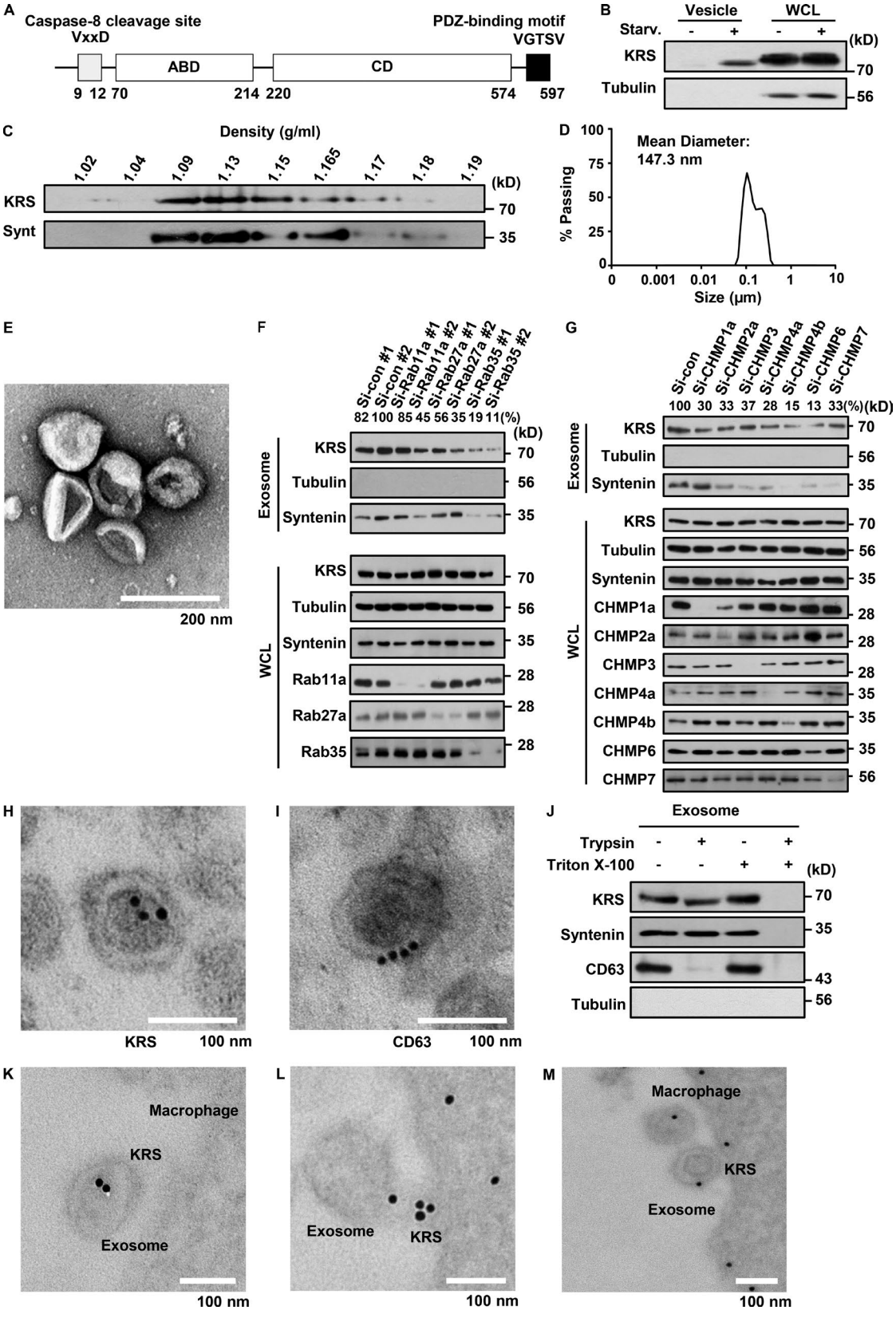

Figure 1. **KRS secretion via exosomes.** (A) Human cytosolic KRS (597 aa) consists of anticodon-binding (ABD; 70–214 aa) and catalytic domains (CDs; 222–574 aa; Guo et al., 2008). The caspase-8 cleavage site (VxxD) and PDZ-binding motif (VGTSV) are located in the N- (9–12 aa) and C-terminal (594–597 aa) ends. (B) HCT116 cells were incubated in normal and starvation (Starv.) conditions for 24 h. The culture media were subjected to ultracentrifugation at 100,000 *g* to obtain the pellet. KRS present in the pellets (containing vesicle fraction) was separated by 8% PAGE and detected by immunoblotting with anti-KRS antibody. Notice a slight difference in the gel mobility of KRS in the medium and cell lysates (see Fig. 3 A for further investigation). (C) Isolated vesicles from B were separated by OptiPrep gradient centrifugation. The nine fractions in the 1.02–1.19 g/ml density range were collected,

rescence complementation (BiFC) assay using green fluorescent Venus protein, where the 173-aa N- and 155-aa C-terminal fragments of Venus were fused to the C-terminal ends of KRS and syntenin, respectively. Interaction of the two proteins would restore Venus green fluorescence. We incubated HCT116 cells expressing the KRS-VN173 and syntenin-VC155 in complete and starvation media and measured the generation of green fluorescence. We observed fluorescence only under starvation conditions (Fig. 2 B and Videos 1, 2, 3, and 4). To determine whether syntenin is required for KRS secretion, we suppressed syntenin with its specific siRNA, which decreased the amount of secreted KRS in a dose-dependent manner (Fig. 2 C) and also decreased the amount of KRS in the isolated exosomes (Fig. 2 D).

To see whether the C-terminal PDZ-binding motif of KRS is critical for syntenin binding and exosomic secretion of KRS, we compared the interaction of KRS WT and the C-terminal 5-aa deleted mutant (ΔC5) with syntenin by coimmunoprecipitation and found that the KRS ΔC5 mutant showed reduced binding to syntenin (Fig. 2 E). We then examined whether the WT and ΔC5 mutant forms of KRS were different in their secretion profiles, and we observed the reduced secretion and exosome incorporation of the KRS ΔC5 mutant (Fig. 2, F and G, respectively). To further validate the importance of the PDZ-binding motif, we introduced alanine substitutions to the four C-terminal residues (C4A mutant; Wieman et al., 2009; Mañes et al., 2010) and monitored how these mutations affected recruitment of KRS into exosomes. The amount of KRS C4A mutant was significantly lower than that of KRS WT in the isolated exosomes (Fig. 2 H). All of these results suggest that syntenin binding to the C-terminal PDZ-binding motif facilitates exosomic secretion of KRS.

The role of the KRS N terminus in secretion

The molecular weight of KRS from isolated exosomes appeared to be smaller than cytosolic KRS, suggesting that a portion of KRS was cleaved off during the secretion process (Figs. 1 B and 3 A). To determine the cleavage site, we expressed N- and C-terminal Myc-tagged KRS in HCT116 cells, isolated secreted exosomes, and performed immunoblot analysis using an anti-Myc antibody. We detected a KRS variant that had Myc fused to the C terminus but not the N terminus (Fig. 3 B), indicating that KRS is cleaved at the N terminus. We also prepared a double-tagged form of KRS in which Strep and Myc tags were fused to the N- and C-terminal ends, respectively, and then we expressed Strep-KRS-Myc fusion protein in HCT116 cells. We detected secreted KRS using the anti-Myc but not the anti-Strep antibody (Fig. 3 C), further supporting that the secreted KRS was cleaved at its N-terminal region. Next, to monitor secretion-induced KRS cleavage, we attached the N- and C-terminal domains of Renilla luciferase (Kerppola, 2008; Ofir-Birin et al., 2013) to the N- and C-terminal ends of KRS, respectively, to measure BiFC of the two Renilla luciferase domains. Whereas intact KRS was expected to bring the two domains of Renilla luciferase into proximity, which would restore luciferase activity, cleavage of KRS would ablate BiFC of the two Renilla luciferase domains. Indeed, upon HCT116 cell starvation, the BiFC signal decreased in a time-dependent manner (Fig. S3 A). We then expressed the GFP-KRS fusion protein in HCT116 cells and incubated the cells under starvation conditions. The presence of cytosolic GFP resulting from cleavage of GFP-KRS showed a similar kinetic pattern to that of KRS secretion (Fig. 3 D). All of these results indicate that KRS cleavage at its N-terminal region is associated with its secretion.

We next determined the exact site of cleavage in KRS. We prepared a series of N-terminal deletion mutants of Myc-KRS and compared the effects of the deletion on KRS secretion. Among the tested mutants, the secretion of KRS mutants ΔN20, ΔN30, and ΔN40 (with the N-terminal 20, 30, and 40 aa deleted, respectively) was observed, but not KRS WT and mutant ΔN10 (Fig. 3 E), suggesting that the N-terminal cleavage occurs between the 11th and 20th residues. We then prepared two more Myc-KRS mutants, ΔN11 and ΔN12, and conducted the same experiments from Fig. 3 E in which we detected Myc-KRS ΔN12 but not ΔN10 and ΔN11 (Fig. 3 F). Collectively, these results suggest that the secretion-associated cleavage occurs at the 12th residue. For further confirmation, we mutated Asp residue at the position of 12 to Ala (D12A) and tested whether this mutation affected the secretion of KRS. The KRS-Myc D12A mutant was not detected in the culture medium, indicating that the mutation significantly reduced the KRS secretion (Fig. 3 G). We also monitored secretion-associated cleavage of this mutant using BiFC Renilla luciferase. The starvation-induced reduction of Renilla luciferase activity was not observed in the D12A mutant (Fig. S3 B). Similarly, the starvation-induced cleavage of GFP-KRS was not observed for the GFP-KRS D12A mutant (Fig. S3 C). When we subjected Myc-KRS WT and the ΔN12 mutant isolated from secreted exosomes to immunoblotting with the anti-Myc antibody, we detected only Myc-KRS ΔN12 but not WT, further indicating that the cleavage occurred at the D12 position (Fig. 3 H). In a comparison of exosome incorporation of KRS-Myc WT and the D12A mutant, only KRS WT was detected in the isolated exosomes, further confirming the importance of D12 cleavage for exosome incorporation and secretion of KRS (Fig. 3 I).

The role of caspase-8–mediated N-terminal cleavage in syntenin interaction

We next determined the enzyme responsible for the cleavage of the N-terminal 12-aa domain of KRS. Interestingly, the

and the presence of KRS and syntenin (Synt) was analyzed by immunoblotting with their specific antibodies. (D) Dynamic light scattering demonstrated the size distribution of the isolated vesicles (mean diameter, 147.3 nm). (E) Negatively stained field of the KRS-containing vesicles isolated from HCT116 cells as in B. (F and G) To see whether Rab (F) and ESCRT-III (G) proteins are involved in the exosomic secretion of KRS, we transfected HCT116 cells with siRNAs specifically targeting each of the indicated Rab and ESCRT-III proteins and examined whether KRS secretion was affected by the suppression of Rab and ESCRT-III proteins. The secretion of KRS was induced by starvation of HCT116 cells for 24 h. After isolation of the secreted exosomes, the amounts of KRS in the obtained exosomes were compared by immunoblotting with anti-KRS antibody. Quantitation of secreted KRS blots was measured by ImageJ. si-con, control siRNA; WCL, whole-cell lysate. (H and I) Localization of KRS (H) and CD63 (I), a known membrane-bound marker for exosomes, was shown by immunogold-staining EM with their respective antibodies. (J) The isolated vesicles were incubated with or without 0.025% trypsin and 0.1% Triton X-100 at 37°C for 30 min, and the presence of KRS, syntenin, and CD63 was analyzed by immunoblotting with their specific antibodies. (K–M) Immunogold-staining EM shows KRS located in the lumen of the exosome near the target macrophage (K), outside of the exosomes near macrophages (L), and within the target macrophage (M).

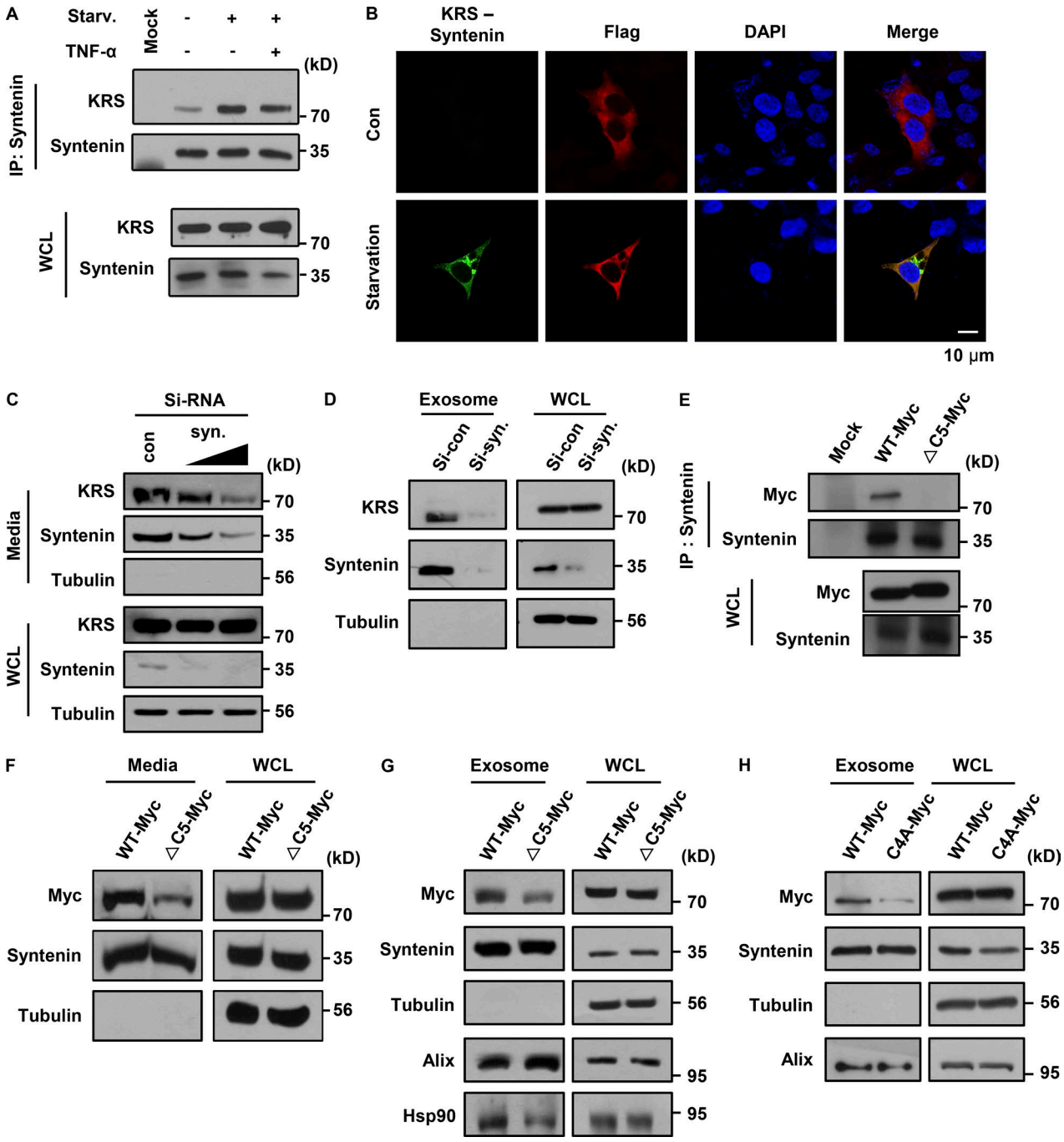

Figure 2. **Interaction of KRS with syntenin for secretion.** (A) HCT116 cells were incubated in the starvation (Starv.) condition in the absence and presence of TNF-α, and the interaction of KRS with syntenin was determined by coimmunoprecipitation with an anti-syntenin antibody. (B) The cellular interaction of KRS and syntenin was determined by BiFC. HCT116 cells were cotransfected with Flag-KRS fused to VN173 (Venus N-terminal domain) and HA-syntenin fused to VC155 (Venus C-terminal domain). The cells were incubated in normal and starvation conditions for 6 h, and reconstitution of Venus green fluorescence was shown by fluorescence microscopy. Expression of KRS was observed by red fluorescence signal from Alexa Fluor 594–conjugated anti-FLAG antibody (60×). Nuclei were visualized by DAPI staining (blue). (C) Secreted KRS and syntenin (syn) were detected by immunoblotting of proteins from HCT116 cells treated with different amounts of siRNA against syntenin. The cells were incubated in starvation conditions for 24 h. Secreted proteins were precipitated with TCA, and the amounts of KRS were determined by immunoblotting. (D) The levels of KRS were also determined, as described in Fig. 1 B, in isolated exosomes and cell lysates of HCT116 cells transfected with siRNA against syntenin. (E) Interaction of KRS-Myc (WT and ΔC5 [C-terminal 5-aa–deleted mutant]) with syntenin was determined by coimmunoprecipitation from HCT116 cells after 1-h incubation in the starvation condition. Syntenin was precipitated from whole-cell lysates (WCLs) with its specific antibody, and the coprecipitated KRS was immunoblotted with anti-Myc antibody. IP, immunoprecipitation (F) Secretion of KRS (WT and ΔC5) from HCT116 cells was determined in the 24-h starvation media as in C. (G) The amounts of KRS WT and ΔC5 were determined by immunoblotting in the exosomes isolated from HCT116 cells incubated in the starvation condition as in Fig. 1 B. (H) KRS mutant in which the last four aa's, GTSV, were changed to alanine (C4A) was constructed. KRS WT and the C4A mutant secretion from HCT116 cells starved for 24 h, as described in Fig. 1 B, was compared.

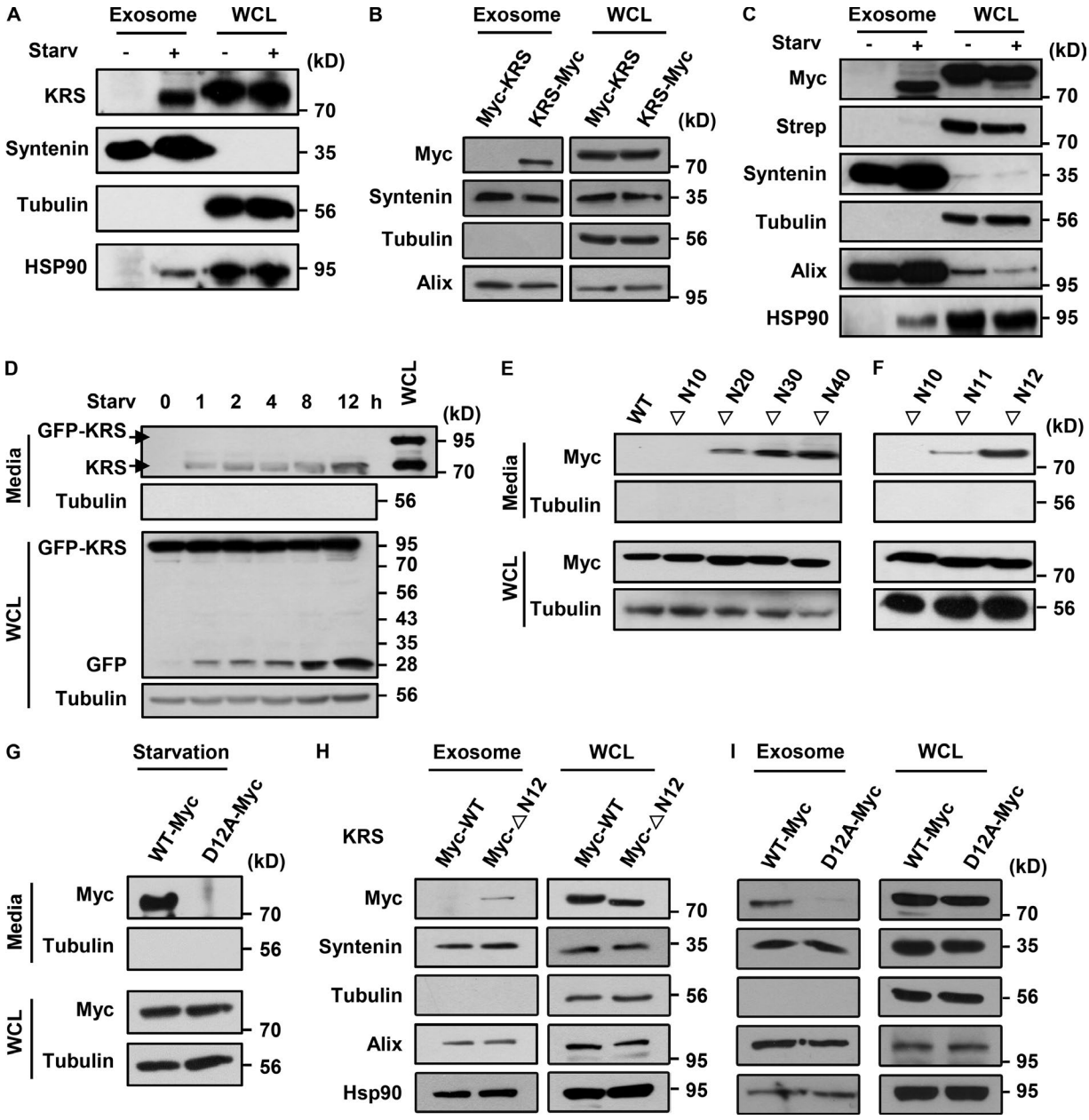

Figure 3. **The effect of an N-terminal truncation of KRS on secretion.** (A) Secreted exosomes were isolated from the complete and starved (Starv) media of HCT116 cells, and KRS in the exosomes and whole-cell lysates (WCLs) was separated by 6% PAGE and detected by immunoblotting. (B) To determine the truncation site, HCT116 cells expressing either Myc-KRS (Myc tag fused to the N-terminal end of KRS) or KRS-Myc (Myc tag fused the C-terminal end of KRS) were incubated in the starvation condition, and the exosomes were isolated from the medium. KRS in the exosomes was detected with anti-Myc antibody. (C) HCT116 cells expressing Strep-KRS-Myc (containing Strep and Myc tags at the N- and C-terminal ends, respectively) were incubated in normal and starvation conditions for 24 h, and KRS in cytosol and exosomes was detected by immunoblotting with anti-Myc and -Strep antibodies, respectively. Syntenin, Alix, and HSP90 were used as markers for exosomes, and tubulin was used for cytosol. (D) HCT116 cells expressing GFP-KRS were incubated in the starvation condition and harvested at indicated time intervals. The amount of GFP-KRS and KRS secreted into the medium and in whole-cell lysates was determined by immunoblotting with anti-KRS and -GFP antibodies, respectively. (E) HCT116 cells expressing each Myc-KRS variant (WT, ΔN10, ΔN20, ΔN30, and ΔN40) were incubated in the starvation medium for 24 h, and the secreted KRS was precipitated with TCA and subjected to immunoblotting with anti-Myc antibody. (F) The same experiments were conducted with Myc-KRS ΔN10, ΔN11, and ΔN12. (G) KRS-Myc WT and D12A mutant proteins were expressed in HCT116 cells, and their secretion was determined by immunoblotting with anti-Myc antibody. (H) Myc-KRS WT and ΔN12 mutant were expressed in HCT116 cells, and their incorporation into the secreted exosomes during 24-h starvation was determined by immunoblotting with anti-Myc antibody. (I) The same experiments were conducted as in H with KRS WT and D12A mutant.

N-terminal peptide of KRS contains a consensus caspase substrate sequence (V-X-X-D, especially for caspase-3, -6, and -8; Fig. 1 A, gray box; Van Damme et al., 2005). To determine whether any of the known caspases is required for N-terminal truncation and secretion of KRS, we treated HCT116 cells with a pan-caspase inhibitor and checked its effect on KRS truncation and secretion. We found that starvation-induced KRS truncation and secretion were significantly inhibited by the inhibitor treatment (Figs. 4 A and S3 D), suggesting the involvement of caspase activity for secretion. To identify the caspase responsi-

ble for the KRS cleavage, we suppressed each of the caspases-3, -6, -8, and -9 with their specific siRNAs and caspase inhibitors and compared their effects on the secretion of KRS. From them, the knockdown and inhibitor of caspase-8 specifically blocked KRS secretion (Figs. 4 B and S3 E). We also observed that KRS levels were reduced in the exosomes isolated from the caspase-8 inhibitor–treated HCT116 cells (Fig. 4 C). We also monitored the effect of the caspase-8 inhibitor on KRS cleavage using a Renilla luciferase–fused KRS and GFP-KRS truncation. The Renilla luciferase activity was reduced by starvation but restored by treatment of the caspase-8 inhibitor (Fig. 4 D). Likewise, starvation-induced GFP-KRS cleavage was inhibited by the treatment of caspase-8 inhibitor (Fig. S3 F).

We next examined whether the expression level of caspase-8 in cells is affected by starvation conditions and found that starvation led to a specific increase in the levels of caspase-8 but not other caspases in a time-dependent manner (Fig. 4 E). We also found that exogenously introduced caspase-8 increased the levels of secreted KRS in a dose-dependent manner (Fig. 4 F). We then investigated whether inhibition of caspase-8 affects the interaction of KRS with syntenin using coimmunoprecipitation and found that the starvation-induced interaction of the two proteins was inhibited by the treatment of the caspase-8 inhibitor (Fig. 4 G). These data suggest the importance of the caspase-8 cleavage of the KRS N-terminal peptide for the interaction of KRS with syntenin. We also compared the interaction of KRS WT and D12A mutant with syntenin by coimmunoprecipitation and found that the interaction of the D12A mutant with syntenin was reduced compared with that of KRS WT (Fig. 4 H). In the BiFC approach of KRS and syntenin described in Fig. 2 B, KRS D12A mutation or the inhibitor treatment inhibited the generation of green fluorescence (Fig. 4 I). Collectively, these experiments identified caspase-8 as the enzyme responsible for the cleavage of KRS at D12, which facilitates the syntenin interaction that promotes its secretion.

Syntenin-dependent dissociation of KRS from multi-tRNA synthetase complex (MSC)

A majority of KRS exists as a component of the cytosolic MSC. We therefore investigated whether the secretion of KRS requires its dissociation from the MSC using gel filtration chromatography. When proteins extracted from HCT116 cells under complete and starvation conditions were subjected to gel filtration, we found that the amount of KRS dissociated from the MSC was increased by starvation, whereas glutamyle-prolyl-tRNA synthetase (EPRS), another component of MSC, was not (Fig. 5 A; Sampath et al., 2004). We then examined whether the N12-aa truncation affected the dissociation of KRS from the MSC. We starved HCT116 cells in the absence and presence of caspase-8 inhibitor and precipitated cellular MSC with an anti-EPRS antibody. The portion of KRS not bound to MSC was detected by immunoblotting of KRS, which remained in the immune-depleted supernatants after removing the immunoprecipitates. KRS in the immune-depleted fraction was decreased in cells treated with the caspase-8 inhibitor (Fig. 5 B), suggesting that caspase-8–mediated N-terminal cleavage of KRS can enhance the dissociation of KRS from MSC. Using the same method, we examined whether the N12 deletion or cleavage-defective D12A mutation would affect the dissociation of KRS from the MSC. In contrast with the KRS WT and ΔN12 mutants, KRS D12A was not detected in immune-depleted supernatants (Fig. 5 C). In addition, knockdown of syntenin reduced the amount of KRS in the immune-depleted fractions. We also compared the starvation-induced dissociation of KRS WT and ΔC5 mutant from MSC as in Fig. 5 B and found that the ΔC5 mutant level was significantly reduced in the immune-depleted fraction (Fig. 5 D). All these results suggest that the caspase-8–mediated N-terminal cleavage of KRS facilitates the trafficking of KRS from the MSC to exosomes via syntenin.

We then investigated whether syntenin can guide KRS to Alix, a known marker for the MVB (Matsuo et al., 2004; Odorizzi, 2006; Baietti et al., 2012) from which exosomes are secreted. For this experiment, we monitored whether the BiFC green fluorescence signals resulting from KRS and syntenin complex formation would colocalize with mCherry-labeled Alix, which emitted red fluorescence. The starvation-induced KRS–syntenin complex colocalized with the mCherry-Alix fraction (Fig. 5 E), suggesting that syntenin can guide the bound KRS from the MSC to the MVB. We examined the presence of KRS in MVBs using immunogold-staining EM with the anti-KRS antibody and found the KRS-specific immunogold particles enriched in the vesicles located within MVBs in HC116 cells grown under starvation conditions (Fig. 5 F).

Inflammatory activity of KRS-harboring exosomes

Previously, we have shown that KRS can trigger inflammatory responses when it was treated with macrophages (Park et al., 2005b). We therefore compared the ability of naked KRS WT, ΔN12 mutant protein, and KRS-containing exosomes to induce various cytokines and factors that are known to be markers for M1- and M2-type macrophages. They showed similar activities in inducing TNF-α, CRG-2, IL6, and MMP9 from RAW264.7 cells (Fig. 6 A), which are the signatures for M1-type macrophages (Mantovani et al., 2002), with EC50 values of 83.4 nM (KRS WT protein), 70.7 nM (KRS ΔN12 mutant), and 2.89 μg/ml (KRS exosome; Fig. S4 A). They also induced macrophage migration (Fig. S4 B). These results suggest that the truncation of the N-terminal 12 aa does not ablate the immune-stimulatory activity of KRS WT and that KRS-containing exosomes are functionally equivalent to naked KRS in their ability to activate M1 polarization of macrophages.

To evaluate the functional significance of KRS in isolated exosomes, we isolated exosomes from HCT116 cells treated with the control and KRS-specific siRNAs (si-KRSs) and compared their ability to induce TNF-α. Knockdown of KRS by its specific siRNA significantly reduced KRS content in exosomes while not affecting exosome content of components such as syntenin and Alix (Fig. 6 B). The exosomes obtained from the si-KRS–treated cells showed reduced TNF-α–inducing and macrophage migration activities compared with those of control siRNA–treated cells (Fig. 6, C and D). To confirm these data in vivo, we monitored the effect of exosomes isolated from cells expressing either the KRS-specific or control siRNAs on the migration of macrophages and neutrophils in vivo. For this experiment, we performed intravital confocal microscopy on GFP-lysozyme (GFP-LysM) transgenic mice in which the mobility of macrophages and neutrophils can be monitored by green fluorescence (Faust et al., 2000; Choe et al., 2013). When we injected the naked KRS (labeled as red fluorescence) in the mouse ear intradermally, we observed that the ability of KRS to attract immune cells was enhanced compared with BSA injection (Fig. S4 C and Videos 5 and 6). We

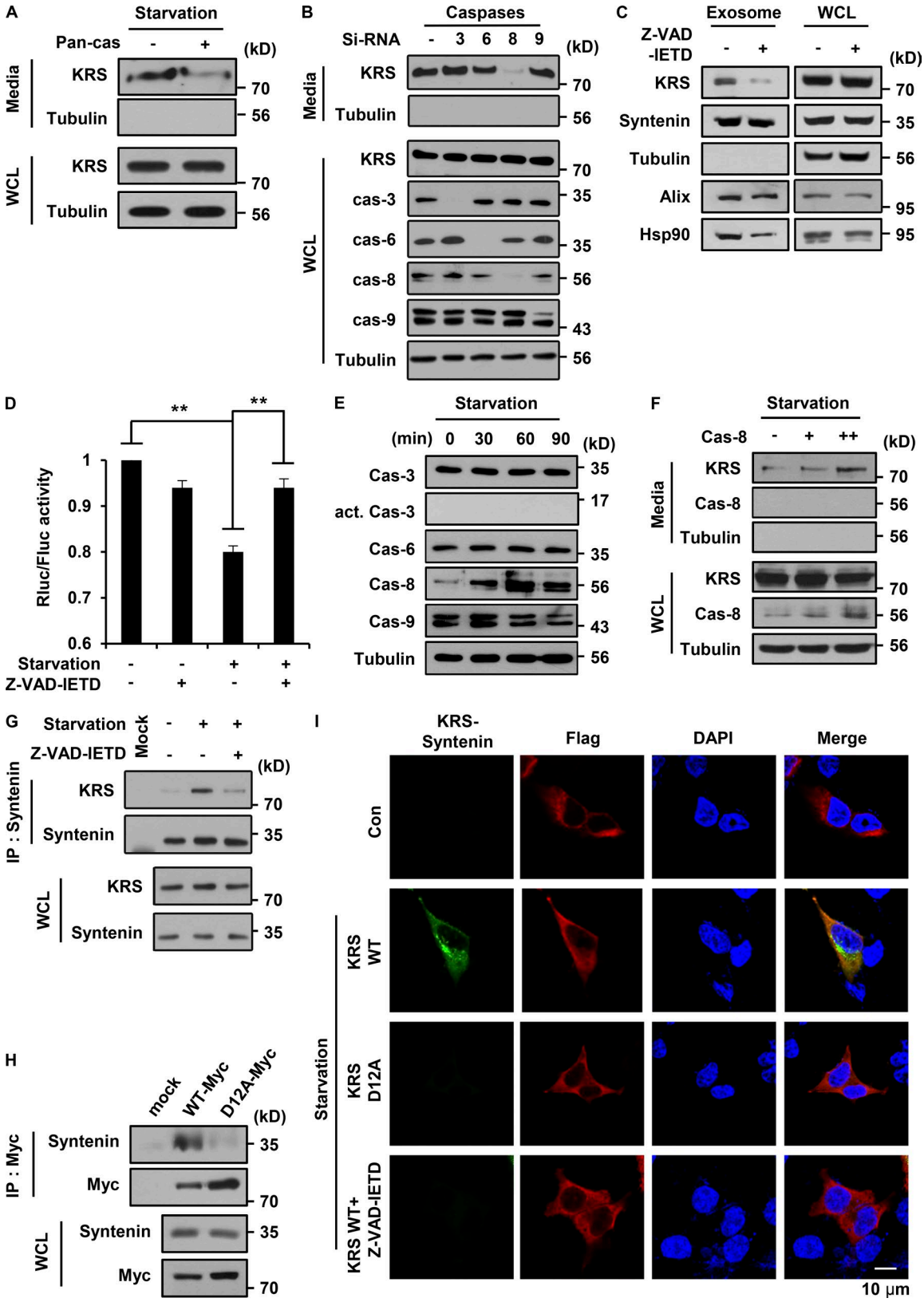

Figure 4. **N-terminal truncation of KRS by caspase-8.** (A) Starved HCT116 cells were treated for 24 h with the pan-caspase (Pan-cas) inhibitor Z-VAD-FMK, and secreted KRS was precipitated with TCA and detected by immunoblotting with anti-KRS antibody. (B) HCT116 cells were transfected with caspase-specific siRNAs, and their effect on KRS secretion was determined by immunoblotting with anti-KRS antibody. (C) The effect of a specific caspase-8 inhibitor, Z-VAD-IETD, on KRS secretion was determined by immunoblotting of isolated exosomes. (D) The effect of the caspase-8 inhibitor on the N-terminal truncation of KRS was determined using KRS containing two domains of Renilla luciferase (Rluc), one fused to each end. Firefly luciferase (Fluc) was used to monitor transfection efficiency. Error bars show means ± SD from a mean of three experiments. $n = 3$. **, $P < 0.01$. (E) The effect of starvation on the

then isolated exosomes from HCT116 cells transfected with the control siRNA and si-KRS, labeled them with red fluorescent DiI, and injected them into GFP-LysM mice. The exosomes isolated from control siRNA–transfected cells induced infiltration of macrophages and neutrophils more strongly than those isolated from cells transfected with si-KRS (Fig. 6, E and F; and Videos 7, 8, and 9). Using the same method, we confirmed that B16F10 cells overexpressing KRS WT–Myc showed more potent immune cell–attracting activity than the EV-transfected control cells. We also observed that cells expressing secretion-defective KRS D12A mutant (Fig. S4 E) showed reduced immune cell–attracting activity compared with those expressing KRS WT (Fig. 6, G and H).

Discussion

Although many ARSs have been reported to be secreted (Son et al., 2014), their secretion pathways have remained unclear. This work is the first study suggesting that ARSs can be secreted via exosomes or exosome-like extracellular vesicles. In addition, our study provides several other findings. First, we found that both of the N- and C-terminal ends of KRS play distinct roles in its secretion. Based on the crystal structure of KRS, which shows that two monomers of KRS exist as an antiparallel homodimer (Ofir-Birin et al., 2013), the N- and C-terminal ends of the two KRS monomers are in close proximity through dimerization. Thus, the N-terminal peptide region of KRS might mask the PDZ-binding motif located in the C-terminal end of its counterpart in trans. Removal of the N-terminal peptide with caspase-8 could expose the C-terminal PDZ-binding motif of the counterpart KRS, which then provides a docking site for syntenin.

This work also suggests a novel mechanism by which KRS dissociates from the MSC. Previously, phosphorylation at T52 and S207 was reported to be responsible for the dissociation of KRS from the MSC for its membrane and nuclear translocation, respectively (Yannay-Cohen et al., 2009; Kim et al., 2012). However, it was not understood how KRS dissociates from the MSC for extracellular secretion. We examined whether phosphorylation is also involved in the dissociation of KRS from the MSC in the process of secretion but did not detect any starvation-induced phosphorylation of KRS (Fig. S5). Instead, this work indicated a novel mechanism for KRS translocation. Namely, KRS dissociation from the MSC and its extracellular secretion involves N-terminal cleavage of KRS by caspase-8 and an interaction with syntenin through its C-terminal end.

The starvation-induced interaction of KRS with syntenin provides strong evidence for the exosomic secretion of KRS (Fig. 2 A), and additional evidence further supports this possibility. First, the biophysical and morphological characteristics of the KRS-containing vesicles are similar to those of typical exosomes (Fig. 1, C–E). Second, KRS was detected in the lumen of the isolated exosomes (Fig. 1, H and J; and Fig. S2 A). Interestingly, the secretion of KRS was reduced by the suppression of different Rab GTPases, although it was most significantly affected by Rab35 (Fig. 1 F). Besides, the KRS secretion was also affected by the suppression of ESCRT-III components that are known to play distinct roles in the secretion pathway of typical exosomes (Fig. 1 G). Although all of these results strongly support the exosomic secretion of KRS, additional investigation appears to be necessary to see whether the KRS exosome would take only one specific route or multiple routes for its secretion.

Interestingly, the amount of HSP90 detected in the isolated exosomes showed a positive correlation with that of KRS (Fig. 3, A and C; and Fig. 4 C). Considering that secreted HSP90 is also known to work as an immune-stimulatory factor (Basu et al., 2000; Bohonowych et al., 2014), it is possible that KRS exerts a synergistic activity with HSP90 and other inflammatory factors present in these exosomes. In fact, we determined that KRS comprised ∼1% of the total exosome proteins (unpublished data). Nonetheless, the exosomes containing even such a low KRS content showed immune-stimulatory activity comparable to the naked KRS at much higher levels (Figs. 6 and S4), supporting the notion that KRS could synergize with other exosome factors in immune cell modulation.

The identification of KRS as a substrate of caspase-8 suggests an unexpected functional connection of the two enzymes. Whereas apoptotic caspases are known to initiate programmed cell death, additional noncanonical activities have been reported (Creagh, 2014; Man and Kanneganti, 2016). Among these, caspase-8 has been shown to trigger inflammation by the activation of pro-IL1β and pro-IL18 (Bossaller et al., 2012; Gringhuis et al., 2012). However, it is unknown whether caspase-8 is also involved in inflammation caused by cancers. This study suggests a novel functional connection between caspase-mediated signaling and a key enzyme for protein synthesis, KRS, which is also active in immune stimulation when secreted into the extracellular space.

Materials and methods

Cell culture and materials

HCT116 cells were cultured in RPMI medium (with 25 mM Hepes buffer and L-glutamine; Hyclone) supplemented with 10% FBS and 50 µg/ml penicillin and streptomycin at 37°C in a 5% CO_2 incubator. RAW264.7 cells were cultured in high-glucose DMEM (with 4 mM L-glutamine, 4.5 mg/ml glucose, and sodium pyruvate; Hyclone) supplemented with 10% FBS and 50 µg/ml penicillin and streptomycin at 37°C in a 5% CO_2 incubator. siRNAs specific to syntenin (SC-42164) and stealth-universal RNAi (SC-37007) were purchased from Santa Cruz Biotechnology, Inc., and those for KRS (HSS105656), caspase-3 (HSS101372), -6 (HSS101378), -8 (HSS141461), -9 (HSS189012), and stealth RNAi Negative Control Medium GC Duplex (253001) were purchased from Invitrogen. Silencer siRNA–targeted CHMP1a (104240), CHMP2a (21469), CHMP3 (148627), CHMP4a (29034), CHMP4b (129910), CHMP6 (140828), CHMP7 (127947), Rab11a (15126 and 120400), Rab27a (12389 and 120391), Rab35 (120486

expression levels of different caspases in HCT116 cells was determined by immunoblotting with their specific antibodies. act., active. (F) Different amounts of caspase-8 were expressed in the starved HCT116 cells, and their dose-dependent effects on secretion of KRS were determined. (G) The effect of the caspase-8 inhibition on the starvation-induced interaction of endogenous KRS and syntenin was determined by coimmunoprecipitation of HCT116 cell lysates using anti-syntenin and anti-KRS antibodies. (H) The effect of the KRS D12A mutation on KRS interaction with syntenin was determined by coimmunoprecipitation. IP, immunoprecipitation. (I) The effect of caspase-8 inhibitor on the cellular interaction of the FLAG-KRS (WT, D12A)–Venus (N domain) and HA-syntenin–Venus (C domain) in starved HCT116 cells was monitored by a BiFC experiment as described in Fig. 2 B (60×).

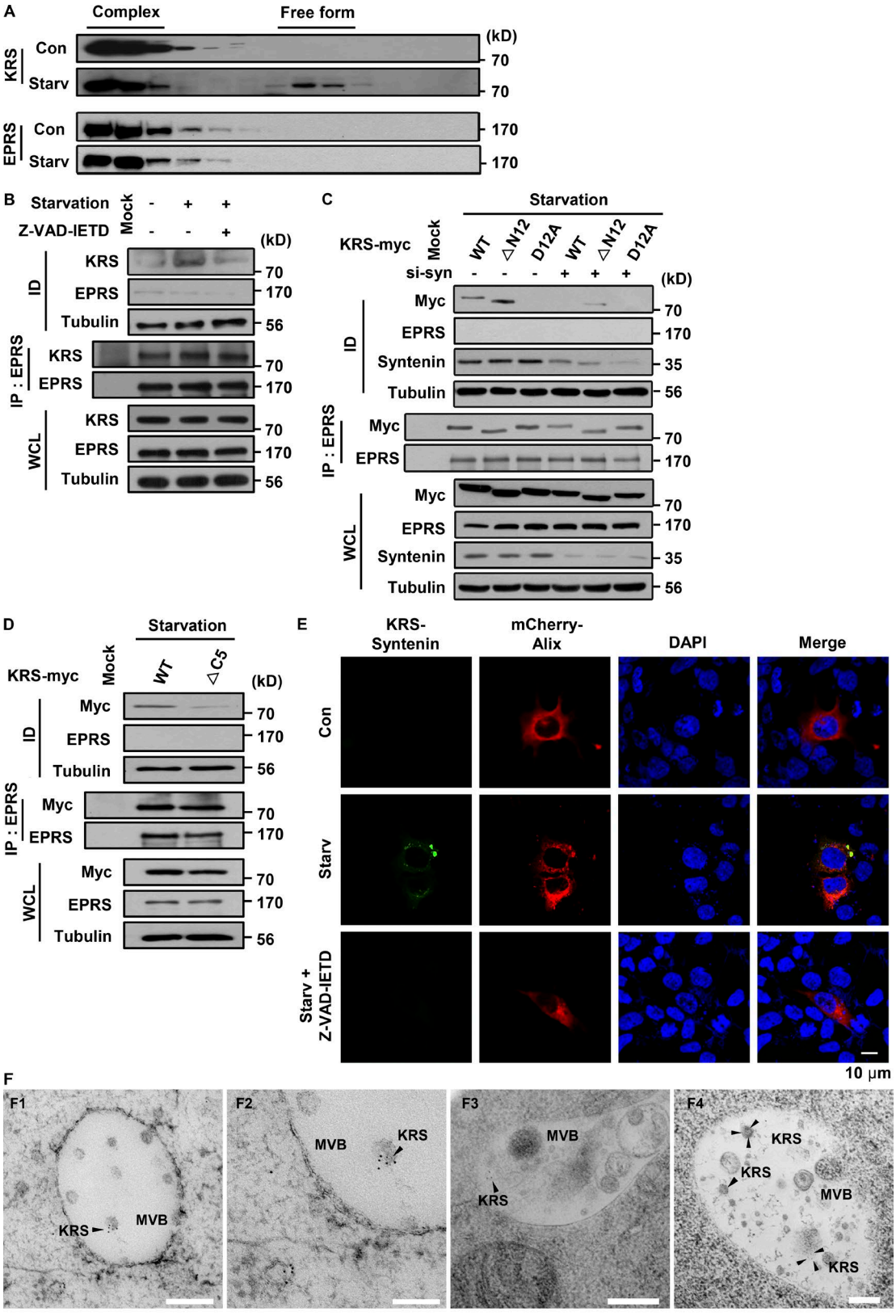

Figure 5. **Translocation of KRS from the MSC to exosomes.** (A) Dissociation of KRS and EPRS from the MSC was monitored by gel filtration of proteins that were extracted from HCT116 cells incubated in normal (control; Con) and starvation (Starv) conditions. EPRS is a known component of MSC (Quevillon et al., 1999). (B) The effect of caspase-8 inhibitor (Z-VAD-ETD) on the starvation-induced dissociation of KRS from MSC in HCT116 cells was determined by coimmunoprecipitation of KRS and EPRS. The proportion of KRS dissociated from MSC was determined by immunoblotting the supernatant (ID) after removing the coimmunoprecipitates of KRS and EPRS (IP). The cellular levels of KRS and EPRS were determined in whole-cell lysates (WCLs). 100% and 15% of IP and ID samples were loaded for gel electrophoresis, respectively. (C) The effects of ΔN12 and D12A mutations and syntenin (syn) knockdown on

and 120487), Silencer Select Negative Control siRNA (43090844 and 43090847), and Silencer Negative control siRNA (AM4635) were purchased from Thermo Fisher Scientific. They were transfected using Lipofectamine 2000 transfection reagent (Invitrogen) and X-tremeGENE HP DNA transfection reagent (Roche) following the manufacturers' protocol. The peptide inhibitors specific to caspase-3 (Z-VAD-DQMD), -6 (Z-VAD-VEID), -8 (Z-VAD-IETD), and -9 (Z-VAD-LEHD) were obtained from EMD Millipore and added to cells at 14 μM in serum-free conditions.

Plasmids

The N- and C-terminal Myc-tagged human KRS proteins were cloned at the EcoRI–XhoI sites of pcDNA3 plasmid. The N-terminal one Strep tag was inserted at the KpnI–BamHI sites of the C-terminal Myc-tagged human KRS plasmid. The N-terminal Myc-tagged human KRS mutants (ΔN10, ΔN20, ΔN30, ΔN40, ΔN11, and ΔN12) and the C-terminal Myc-tagged human KRS mutants (ΔC5) were cloned at the EcoRI–XhoI sites of the pcDNA3 plasmid. pEGFP-KRS and the BiFC plasmids of pBiFC-VN173 (FLAG tag) and pBiFC-VC155 (HA tag) were previously described (Kwon et al., 2011; Kim et al., 2012). pBiFC-VN173-KRS and –VC155-syntenin were cloned at the HindIII–XbaI (KRS) and EcoRI–EcoRI (syntenin) sites of pBiFC plasmids. The BiFC N-terminal Renilla-KRS–C-terminal Renilla plasmid was a gift from M. Guo (The Scripps Research Institute, Jupiter, FL). pmCherry-Alix plasmid was cloned at the EcoRI–BamHI sites of pmCherry-C1 plasmid. The cDNAs encoding Myc-KRS, KRS-Myc, and the pBiFC-VN173-KRS mutant at D12A, C4A were cloned using a QuikChange II kit (Agilent Technologies) following the manufacturer's instructions.

Immunoblotting and immunoprecipitation

Cells were lysed with 50 mM Tris-HCl buffer, pH 7.4, containing 150 mM NaCl, 10 mM NaF, 1 mM EDTA, 1% NP-40, 10% glycerol, and protease inhibitor. After 30 min, the supernatants were dissolved in SDS sample buffer and separated by SDS-PAGE. Antibodies against different ARSs were used for immunoblotting (Abcam). Antibodies specific to Hsp90 (H-114), syntenin (S-31), CD63 (H-193), Rab11a (A-6), Rab27a (E12A-1), Rab35, CHMP1a (B-5), CHMP3 (FL-222), CHMP4a (H-52), CHMP6 (B-3), GFP (B-2), Myc (9E10), caspase-3 (E-8), -6 (H-12), -8 (4.1.20), -9 (H-83), and HIF1-α (H-206) were purchased from Santa Cruz Biotechnology, Inc.; Rab35 and CHMP7 antibodies were purchased from Novus Biologicals. CHMP4b antibody was purchased from Proteintech. Those for Alix (3A9), BIP (C50B12), p-S6K (Thr398; 9205), S6K (9202), p-tyrosine (9411), p-threonine (9381), and IRE1-α (14C10) were purchased from Cell Signaling Technology; p-IRE1–α (Ser724) was purchased from Novus Biologicals; and p-serine (p3430) and β-actin (A5441) were purchased from Sigma-Aldrich. Active caspase-3 (C92-605) was purchased from BD. For immunoprecipitation, cells were lysed at 4°C in 50 mM Hepes buffer, pH 7.4, containing 150 mM NaCl, 0.5% NP-40, 2 mM EDTA, 5% glycerol, and protease inhibitor (EMD Millipore). The protein extracts were incubated with specific antibody for 2 h at 4°C with agitation, and then protein G Agarose was added and further incubated for 4 h. After centrifugation, the precipitated samples were resuspended in cold lysis buffer and washed three times. Proteins were eluted from the beads and separated by SDS-PAGE.

Determination of KRS secretion

HCT116 cells were cultivated to 60% confluency in RPMI containing 10% FBS. After cells were washed twice, they were transferred to serum-free RPMI for 24 h. The culture media were collected and centrifuged at 500 *g* for 10 min. The supernatants were centrifuged again at 10,000 *g* for 30 min to eliminate membrane organelles, and then proteins were precipitated with 12% TCA and incubated for 12 h at 4°C. Pellets were obtained by centrifugation at 18,000 *g* for 15 min and neutralized with 100 mM Hepes, pH 8.0. Proteins in the pellets were separated by SDS-PAGE and subjected to immunoblotting with an anti-KRS antibody.

Exosome isolation

Media were obtained from HCT116 cells incubated in the complete (RPMI containing 10% FBS) and starvation (RPMI only) conditions and subjected to centrifugation at 500 *g* for 10 min to remove cells and subsequently at 10,000 *g* for 30 min to remove debris. The supernatants were then centrifuged at 100,000 *g* for 1.5 h to precipitate exosomes. Protein content of the isolated exosomes was quantified by a Bradford assay.

OptiPrep density gradient assay and dynamic light scattering

Purified exosomes were loaded onto continuous OptiPrep Density Gradient Medium (40, 20, 10, and 5% iodixanol solution with 0.25 M sucrose and 10 mM Tris-HCl, pH 7.5; Sigma-Aldrich) and centrifuged at 150,000 *g* for 15 h. The 10 fractions were harvested, and proteins in each fraction were obtained by TCA precipitation. Proteins of interest were detected by immunoblot analysis. The size of the secreted vesicles was measured by an ELS-Z light scattering spectrophotometer (Otsuka Electronics).

Gel filtration chromatography

HCT116 cells were lysed with 10 mM Hepes buffer, pH 7.4, containing 10 mM KCl, 100 μM EDTA, 1 mM DTT, 0.4% NP-40, and protease inhibitor mixture. Cell lysates were centrifuged at 13,000 rpm for 15 min, and the supernatants were then transferred to a new tube. The supernatants (4 mg total proteins in 400 μl) were injected into a Superdex200 chromatography column 10/300 GL (GE Healthcare) in an ÄKTA fast protein liquid chromatography system (GE Healthcare). The separated proteins were then resolved by SDS-PAGE and subjected to immunoblotting with antibodies specific to the indicated proteins.

Preparation of human full-length and truncated KRS

The cDNAs for human cytosolic KRS (1–597 aa WT and N-terminal 12 aa truncated) were subcloned into pET-28a (Novagen) with EcoRI and XhoI and expressed in *Escherichia coli* BL21 (DE3). His-tagged KRS was then purified using nickel affinity (Invitrogen) and Mono Q ion-exchange (GE Healthcare) chromatography following the manufacturer's instructions. To remove lipopolysaccharide, the KRS solution was dialyzed in pyrogen-free buffer and subsequently filtered

the dissociation of KRS-Myc from MSC were determined as in B. (D) The effects of ΔC5 (the C-terminal 5-aa deletion) on the dissociation of KRS-Myc from the MSC were determined as in B. (E) The effect of caspase-8 inhibitor on the association and colocalization of KRS-syntenin-Alix was shown by BiFC and fluorescence microscopy, respectively. The starvation-induced association of KRS and syntenin was shown by BiFC (green) as described in Fig. 2 B. The localization of KRS–syntenin complexes revealed by BiFC was further analyzed with mCherry-Alix (red). Nuclei were visualized by DAPI staining (blue). (F) Immunogold-staining EM analysis showing the localization of KRS in vesicles located within the MVB of HCT116 cells under starvation conditions. Arrowheads in each panel indicate the localization of immunogold-labeled KRS. Bars: (F1, F3, and F4) 200 nm; (F2) 100 nm.

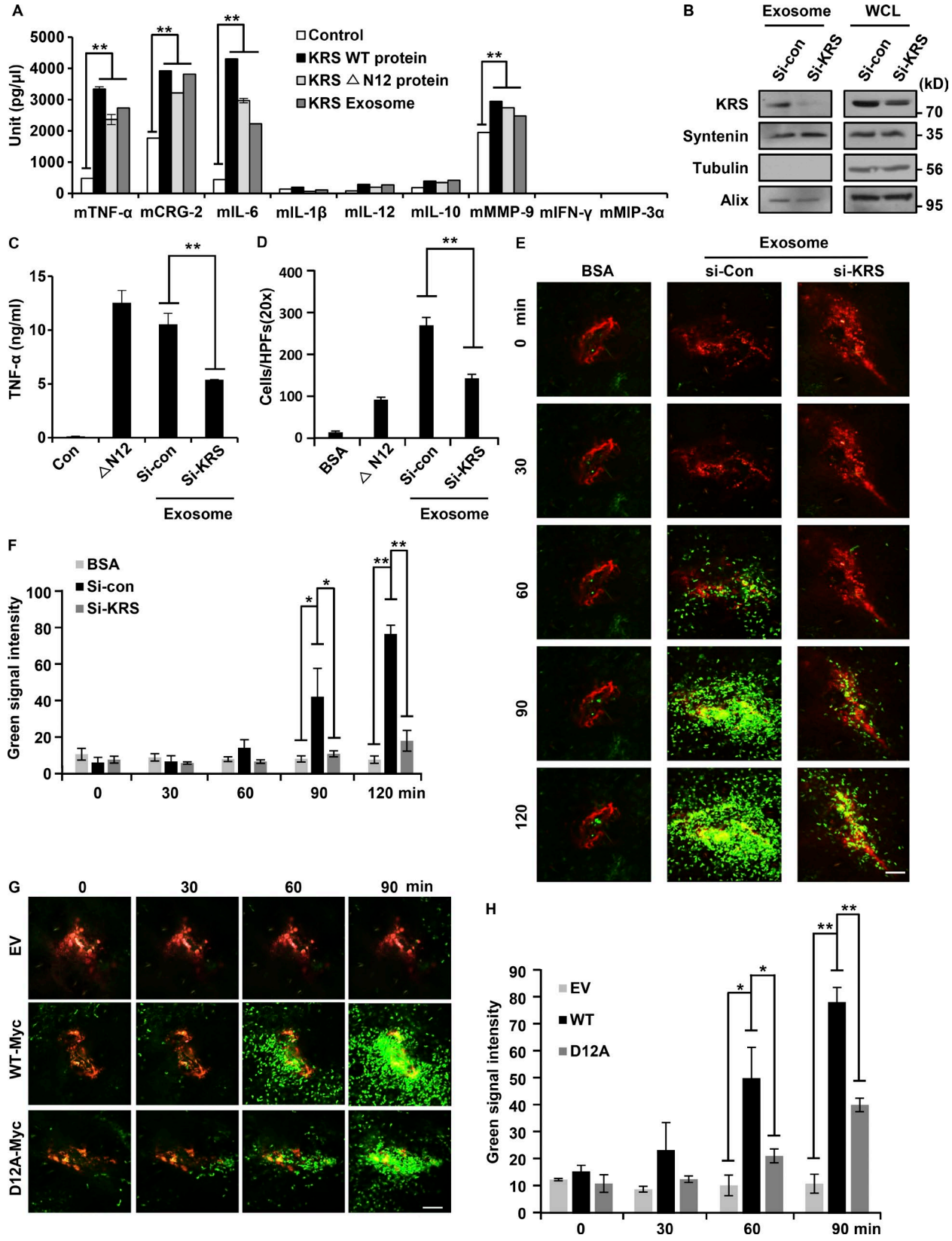

Figure 6. **Biological activities of KRS-containing exosomes.** (A) Effects of KRS WT (6 µg), ΔN12 (6 µg), and KRS exosomes (5 µg by total proteins) on the secretion of the indicated factors from RAW264.7 cells were determined using a multiplex bead array. (B) To assess the functional importance of KRS for exosomes, we reduced the KRS level in exosomes by siRNA knockdown and confirmed by immunoblotting. (C and D) TNF-α–inducing (C) and transwell migration (D) activities of RAW264.7 cells were compared for purified KRS ΔN12 mutant (6 µg) and exosomes (normal and KRS suppressed; 5 µg total proteins) obtained from HCT116 cells. HPF, high-power field. (E) Exosomes (normal and KRS suppressed; 0.1 µg/µl) from HCT116 cells and BSA were stained with DiI (Potter et al., 1996) and Alexa Fluor 647, respectively (red fluorescence), and injected into mouse ear dermis. To visualize macrophage/

through Acrodisc Units with Mustang E membrane, (0.2 µm, 25 mm; Pall Corporation) in PBS containing 20% glycerol.

TNF-α ELISA assay

RAW264.7 cells (2×10^4) were cultured on 24-well plates containing DMEM with 10% FBS and 1% antibiotics for 12 h and then treated with the purified KRS at the indicated concentrations for 6 h. The media were harvested after centrifugation at 3,000 *g* for 5 min, and the secreted TNF-α was measured using a TNF-α ELISA kit (BD) following the manufacturer's instructions.

BiFC immunofluorescence staining

HCT116 cells expressing KRS-VN173, syntenin-VC155, and mCherry-Alix were incubated in starvation conditions with or without caspase-8 inhibitor. The cells were fixed on 9-mm coverslips with 4% paraformaldehyde and permeabilized with 0.1% Triton X-100 for 5 min and then washed briefly with cold PBS. After a 10-min incubation with the CAS-Block (Invitrogen) for blocking, the cells were incubated for 1 h with an anti-FLAG antibody. Alexa Fluor 555 (Invitrogen) was then added for 1 h at room temperature, and cells were DAPI stained for 10 min. After washing with cold PBS for 30 min, the specimens were observed by laser-scanning microscopy. The mounted samples were visualized at room temperature by a confocal fluorescence microscope (A1 Rsi) through an objective lens (Plan Apochromat VC 60×) and with NIS-Elements AR3.2 64-bit software (Nikon). For live-cell time-lapse microscopy, HCT116 cells expressing KRS-VN173 and syntenin-VC155 were seeded in a glass-bottomed two-well imaging chamber (Lab-Tek II; Thermo Fisher Scientific) containing RPMI with 10% FBS and incubated using an On-Stage Cell Incubation system (Live Cell Instrument) at 37°C with 5% CO_2 for 12 h. Cells were then starved for 3 h at 37°C, and images were collected at 3-min intervals. The samples were visualized by confocal fluorescence microscopy (A1 Rsi; Nikon) through an objective lens (Plan Apochromat VC 20× 0.75 NA; Nikon) and an electron-multiplying charge-coupled device camera (iXon; DU897E BV; Andor).

Wound-healing migration assay

RAW246.7 cells (4×10^4) were seeded in 12-well cell culture plates in complete growth media and then incubated until a confluent monolayer was formed. The monolayer of cells was wounded by manual scratching with a pipette tip and washed with PBS, and then media containing either KRS WT, ΔN12 (6 µg/ml) protein, or KRS exosomes (0.05, 0.5, and 5 µg/ml) were added. After 12 h, the wound regions were photographed by phase-contrast microscopy (C1; Nikon) through an objective lens (Plan Apochromat 10×) electron-multiplying charge-coupled device camera (DU-897; Andor) and with NZS-C4.11 software (Nikon).

Transwell migration assay

A 24-well plate transwell chamber with 5.0 µm polycarbonate membrane (Costar) was used for cell migration assays. The inserts were coated with 10 µl of 0.5 mg/ml of gelatin (Sigma-Aldrich) and dried overnight under UV light. RAW264.7 cells were cultured in the bottom chamber. After 12 h, culture media were changed to serum-free DMEM, added to the inserts (10^5 cells), and treated with BSA (100 nM), KRS protein (6 µg/ml), and KRS exosomes (5 µg/ml) purified from HCT116 cells treated with control siRNA or si-KRS for 8 h at 37°C in a 5% CO_2 incubator. The inserts were washed twice with cold PBS, and the cells were fixed in 70% methanol and 30% PBS solution for 30 min. After washing the inserts with PBS three times, the cells were fixed using hematoxylin (Sigma-Aldrich) for 30 min. The inserts were washed with distilled water three times, and the nonmigrant cells were removed with a cotton swab. The membranes were extracted using a blade and mounted to a microslide using GelMount (Biomeda). Images of the migrating cells were taken with an optical microscope (20×; Korea Lab Tech) using the TopView 3.5 software.

Intravital imaging

A custom-built laser-scanning confocal microscope modified from a previously constructed system (Choe et al., 2013) was used to visualize macrophage/neutrophil recruitment. Three continuous wave lasers at 488 nm (MLD488 60 mW), 561 nm (Jive 50 mW), and 640 nm (MLD640 100 mW; Cobolt) were used as excitation sources. To implement 2D scanning, a fast-rotating polygonal mirror (MC-5; aluminum coated; Lincoln Laser) and galvanometer (6230H; Cambridge Technology) were used. High-sensitivity photomultiplier tubes (R9110; Hamamatsu Photonics) were used to detect three-color fluorescence signals simultaneously. Three detection channels were split by dichroic mirrors (FF01-442/46-25, FF02-525/50-25, FF01-585/40-25, and FF01-685/40-25) and bandpass filters (FF484-FDi01, FF560-Di01, and FF649-Di01; Semrock). Electric signals obtained from photomultiplier tubes were digitized by an 8-bit three-channel frame grabber (Solios; Matrox). The field of view of images obtained by the 20× objective (LUMFLN60XW; NA1.1; Olympus) was 500×500 µm^2. After acquisition from the imaging system, 512×512–pixel images were then XY-shift compensated with MATLAB (MathWorks). During the imaging, a motorized XYZ translational stage (MPC-200-ROE; Sutter Instrument), which has 1-µm resolution, was used to precisely adjust sample position.

GFP-LysM mice (Faust et al., 2000) that endogenously express GFP in macrophages and neutrophils were used. 12–20-wk-old male GFP-LysM mice were deeply anaesthetized with intraperitoneal injections of zoletil (30 mg/kg) and rompun (10 mg/kg). During imaging, mouse body temperature was maintained at 37°C with a homoeothermic controller (PhysioSuite; RightTemp; Kent Scientific). To avoid immune responses caused by hair removal, mouse ear skin was shaved at least 12 h before imaging.

B16F10 cells were transfected with myc-KRS, KRS-Myc (WT and D12A Mutant), and empty vector using Lipofectamine 2000 (Invitrogen). The transfected B16F10 cells were then fluorescently labeled with the lipophilic fluorescent dye, Vybrant DiI, or DiD solution (Thermo Fisher Scientific) by incubating with 5 µl DiI or DiD solution per ml of cell media for 1 h. After washing with PBS three times, labeled cells were prepared in PBS solution and intradermally injected into mouse ear skin (4×10^4 cells/µl) with a 31-G microinjector. To visualize macrophage/neutrophil recruitment along the cell injection site, time-lapse images were taken at 30-s intervals after injection.

HCT116 cells were transfected with control siRNA and si-KRS using X-tremeGENE HP DNA transfection reagent (Roche) following

neutrophil (green fluorescence) recruitment to the injection sites, time-lapse intravital images of macrophage/neutrophil (green fluorescence) recruitment were taken in 30-s intervals up to 120 min after injection. (F) These experiments were repeated three times, and the results are represented as bar graph. Green fluorescence signal was measured by ImageJ. (G) B16F10 cells expressing empty vector (EV), KRS WT, and D12A mutant were stained with DiD (Sutton et al., 2008) and injected into mouse ear dermis (4×10^4 cells/µl; red fluorescence). Bars, 100 µm. (H) These experiments were repeated three times, and the results are shown as bar graph. Green fluorescence signal was measured by ImageJ. Error bars show means ± SD from the mean of three independent experiments. $n = 3$. *, $P < 0.05$; **, $P < 0.01$.

the manufacturer's protocol. The transfected HCT116 cells were incubated with DiI (5 µl/ml) for 1 h. After washing with PBS, the labeled cells were incubated in starvation condition for 24 h. Control siRNA and si-KRS exosomes were purified from incubation media using the exosome isolation method described in the Exosome isolation section. Exosomes were intradermally injected into mouse ear skin (0.1 µg/µl) with a 31-G microinjector. Time-lapse images were taken at 30-s intervals after injection.

Luminex screening assays (bead-based multiplex kits)

RAW246.7 cells were cultured in 12-well plates in DMEM with 10% FBS and 1% antibiotics for 12 h and then starved in serum-free media for 2 h. Different amounts of KRS (WT and ΔN12 mutant; 6 µg/ml) and KRS exosomes (5 µg/ml) were added to the media. At different time intervals, the media were collected and subjected to centrifugation at 3,000 *g* for 10 min. For the multiplex assay, the secretion of TNF-α, mCRG-2, IL-6, mIL-1b, mIL-12, mIL-10, MMP9, IFN-γ, mMIP3a, and CXCL10 was measured using premixed beads purchased from R&D Science following manufacturer's instructions and quantified by the Bioplex 200 system and software (Bio-Rad Laboratories).

Renilla luciferase BiFC assay

BiFC Renilla luciferase KRS vector (provided by M. Guo), with which the N- and C-terminal domains of Renilla luciferase were fused to the N- and C-terminal ends of KRS, was cotransfected into HCT116 cells along with the firefly luciferase vector. After 24 h, cells were incubated in each starvation condition with or without caspase-8 inhibitor. Luciferase activity was measured using a luciferase assay kit (Promega) and luminometer.

Immunogold-label EM

Exosomes were isolated from starved HCT116 cells, and exosome-treated macrophages were fixed with 2.5% glutaraldehyde and 2% osmium tetroxide for 1 h at 4°C. They were then dehydrated with a graded acetone series and embedded into Spurr's medium (Electron Microscopy Sciences). The sections were made in 60-nm thickness horizontally to the plane of the samples using an ultramicrotome (RMC MTXL) and then mounted on nickel grids. Free aldehyde groups were quenched with 0.02 M glycine for 10 min. Sections were then rinsed in deionized water, floated for 1 h in PBS containing 1% BSA, and incubated directly in the primary rabbit antibodies at 4°C for 1 h. Sections were rinsed several times with PBS-BSA (0.1% BSA in PBS) and floated for 1 h in rabbit IgG conjugated to 10-nm gold particles (Sigma-Aldrich) diluted 1:50 in PBS-BSA. The gold particle–labeled sections were counterstained with uranyl acetate and lead citrate. For immunogold staining of KRS in MVB, HCT116 cells were incubated in serum-free RPMI 1640 medium for 3 h, and then cells were collected by low-speed centrifugation.

After the preparative steps of cryofixation (Donohoe et al., 2007), the prepared sections were examined using a transmission electron microscope (H-7600; Hitachi) operating at 80 k and a JEM-1400 PLUS transmission electron microscope (JEOL).

Statistical methods

The Student's *t* test was used for statistical analysis. P-values <0.05 was considered statistically significant.

Online supplemental material

Fig. S1 shows KRS and other ARS secretion in different conditions and cell lines. Fig. S2 shows the determination of KRS locations in the secreted exosomes and macrophages using EM. Fig. S3 shows starvation-induced KRS truncation at D12 by caspase-8. Fig. S4 shows the inflammatory activity of secreted KRS exosomes. Fig. S5 shows the effect of starvation on the phosphorylation of KRS. Video 1 shows BiFC live imaging of the KRS and syntenin interaction in normal conditions. Video 2 shows a merge of Video 1. Video 3 shows BiFC live imaging of the KRS and syntenin interaction in starvation conditions. Video 4 shows a merge of Video 3. Video 5 shows intravital images of a BSA-induced macrophage/neutrophil migration. Video 6 shows intravital images of KRS-induced macrophage/neutrophil migration. Video 7 shows time-lapse intravital microscopy of the recruitment of macrophages/monocytes (green) toBSA stained with Alexa Fluor 647. Video 8 shows time-lapse intravital microscopy of the recruitment of macrophages/monocytes (green) to exosomes isolated from starved HCT116 cells that were treated with control siRNA stained with DiI (red fluorescence). Video 9 shows time-lapse intravital microscopy of the recruitment of macrophages/monocytes (green) to exosomes isolated from starved HCT116 cells that were treated with si-KRS stained with DiI (red fluorescence).

Acknowledgments

We thank Professor Min Guo for BiFC Renilla luciferase plasmid.

This work was supported by the Global Frontier Project grants NRF-M3A6A4-2010-0029785 (to S.B. Kim), NRF-M1AXA002-2012M3A6A4054261 (to P. Kim), and NRF-2015M3A6A4065729 (to H.S. Jung) of the National Research Foundation supported by the Ministry of Science, ICT and Future Planning of South Korea.

The authors declare no competing financial interests.

Author contributions: S.B. Kim and H.R. Kim designed the project. S.B. Kim designed experiments, acquired and analyzed data, and drafted the original manuscript. M.C. Park, P.C. Goughnour, D. Han, S. Cho, Y. Kim, I. Yoon, and T. Kang acquired experimental data. E. Song and P. Kim acquired and analyzed LysM mouse data. C. Song, S. Lee, H.S. Jung, H. Choi, and J.Y. Mun performed the immunogold-label EM experiment and acquired and analyzed the data. S. Kim contributed to direct supervision, experimental planning, manuscript writing, review, and editing.

Submitted: 30 May 2016
Revised: 5 October 2016
Accepted: 4 May 2017

References

Baietti, M.F., Z. Zhang, E. Mortier, A. Melchior, G. Degeest, A. Geeraerts, Y. Ivarsson, F. Depoortere, C. Coomans, E. Vermeiren, et al. 2012. Syndecan–syntenin–ALIX regulates the biogenesis of exosomes. *Nat. Cell Biol.* 14:677–685. http://dx.doi.org/10.1038/ncb2502

Barchowsky, A., L.R. Klei, E.J. Dudek, H.M. Swartz, and P.E. James. 1999. Stimulation of reactive oxygen, but not reactive nitrogen species, in vascular endothelial cells exposed to low levels of arsenite. *Free Radic. Biol. Med.* 27:1405–1412. http://dx.doi.org/10.1016/S0891-5849(99)00186-0

Basu, S., R.J. Binder, R. Suto, K.M. Anderson, and P.K. Srivastava. 2000. Necrotic but not apoptotic cell death releases heat shock proteins, which deliver a partial maturation signal to dendritic cells and activate the NF-κB pathway. *Int. Immunol.* 12:1539–1546. http://dx.doi.org/10.1093/intimm/12.11.1539

Bohonowych, J.E., M.W. Hance, K.D. Nolan, M. Defee, C.H. Parsons, and J.S. Isaacs. 2014. Extracellular Hsp90 mediates an NF-κB dependent inflammatory stromal program: Implications for the prostate tumor microenvironment. *Prostate.* 74:395–407. http://dx.doi.org/10.1002/pros.22761

Bossaller, L., P.I. Chiang, C. Schmidt-Lauber, S. Ganesan, W.J. Kaiser, V.A. Rathinam, E.S. Mocarski, D. Subramanian, D.R. Green, N. Silverman, et al. 2012. Cutting edge: FAS (CD95) mediates

noncanonical IL-1β and IL-18 maturation via caspase-8 in an RIP3-independent manner. *J. Immunol.* 189:5508–5512. http://dx.doi.org/10.4049/jimmunol.1202121

Choe, K., Y. Hwang, H. Seo, and P. Kim. 2013. In vivo high spatiotemporal resolution visualization of circulating T lymphocytes in high endothelial venules of lymph nodes. *J. Biomed. Opt.* 18:036005. http://dx.doi.org/10.1117/1.JBO.18.3.036005

Choi, J.W., D.G. Kim, A.E. Lee, H.R. Kim, J.Y. Lee, N.H. Kwon, Y.K. Shin, S.K. Hwang, S.H. Chang, M.H. Cho, et al. 2011. Cancer-associated splicing variant of tumor suppressor AIMP2/p38: Pathological implication in tumorigenesis. *PLoS Genet.* 7:e1001351. http://dx.doi.org/10.1371/journal.pgen.1001351

Creagh, E.M. 2014. Caspase crosstalk: integration of apoptotic and innate immune signalling pathways. *Trends Immunol.* 35:631–640. http://dx.doi.org/10.1016/j.it.2014.10.004

Donohoe, B.S., B.H. Kang, and L.A. Staehelin. 2007. Identification and characterization of COPIa- and COPIb-type vesicle classes associated with plant and algal Golgi. *Proc. Natl. Acad. Sci. USA.* 104:163–168. http://dx.doi.org/10.1073/pnas.0609818104

Fabre, S., C. Reynaud, and P. Jalinot. 2000. Identification of functional PDZ domain binding sites in several human proteins. *Mol. Biol. Rep.* 27:217–224. http://dx.doi.org/10.1023/A:1011008313677

Faust, N., F. Varas, L.M. Kelly, S. Heck, and T. Graf. 2000. Insertion of enhanced green fluorescent protein into the lysozyme gene creates mice with green fluorescent granulocytes and macrophages. *Blood.* 96:719–726.

Gringhuis, S.I., T.M. Kaptein, B.A. Wevers, B. Theelen, M. van der Vlist, T. Boekhout, and T.B. Geijtenbeek. 2012. Dectin-1 is an extracellular pathogen sensor for the induction and processing of IL-1β via a noncanonical caspase-8 inflammasome. *Nat. Immunol.* 13:246–254. http://dx.doi.org/10.1038/ni.2222

Guo, M., and P. Schimmel. 2013. Essential nontranslational functions of tRNA synthetases. *Nat. Chem. Biol.* 9:145–153. http://dx.doi.org/10.1038/nchembio.1158

Guo, M., M. Ignatov, K. Musier-Forsyth, P. Schimmel, and X.L. Yang. 2008. Crystal structure of tetrameric form of human lysyl-tRNA synthetase: Implications for multisynthetase complex formation. *Proc. Natl. Acad. Sci. USA.* 105:2331–2336. http://dx.doi.org/10.1073/pnas.0712072105

Guo, M., P. Schimmel, and X.L. Yang. 2010. Functional expansion of human tRNA synthetases achieved by structural inventions. *FEBS Lett.* 584:434–442. http://dx.doi.org/10.1016/j.febslet.2009.11.064

Han, J.M., S.G. Park, B. Liu, B.J. Park, J.Y. Kim, C.H. Jin, Y.W. Song, Z. Li, and S. Kim. 2007. Aminoacyl-tRNA synthetase-interacting multifunctional protein 1/p43 controls endoplasmic reticulum retention of heat shock protein gp96: Its pathological implications in lupus-like autoimmune diseases. *Am. J. Pathol.* 170:2042–2054. http://dx.doi.org/10.2353/ajpath.2007.061266

Hsu, C., Y. Morohashi, S. Yoshimura, N. Manrique-Hoyos, S. Jung, M.A. Lauterbach, M. Bakhti, M. Grønborg, W. Möbius, J. Rhee, et al. 2010. Regulation of exosome secretion by Rab35 and its GTPase-activating proteins TBC1D10A–C. *J. Cell Biol.* 189:223–232. http://dx.doi.org/10.1083/jcb.200911018

Ibba, M., and D. Soll. 2000. Aminoacyl-tRNA synthesis. *Annu. Rev. Biochem.* 69:617–650. http://dx.doi.org/10.1146/annurev.biochem.69.1.617

Kerppola, T.K. 2008. Bimolecular fluorescence complementation (BiFC) analysis as a probe of protein interactions in living cells. *Annu. Rev. Biophys.* 37:465–487. http://dx.doi.org/10.1146/annurev.biophys.37.032807.125842

Kim, D.G., J.W. Choi, J.Y. Lee, H. Kim, Y.S. Oh, J.W. Lee, Y.K. Tak, J.M. Song, E. Razin, S.H. Yun, and S. Kim. 2012. Interaction of two translational components, lysyl-tRNA synthetase and p40/37LRP, in plasma membrane promotes laminin-dependent cell migration. *FASEB J.* 26:4142–4159. http://dx.doi.org/10.1096/fj.12-207639

Kim, D.G., J.Y. Lee, N.H. Kwon, P. Fang, Q. Zhang, J. Wang, N.L. Young, M. Guo, H.Y. Cho, A.U. Mushtaq, et al. 2014. Chemical inhibition of prometastatic lysyl-tRNA synthetase-laminin receptor interaction. *Nat. Chem. Biol.* 10:29–34. http://dx.doi.org/10.1038/nchembio.1381

Kwon, N.H., T. Kang, J.Y. Lee, H.H. Kim, H.R. Kim, J. Hong, Y.S. Oh, J.M. Han, M.J. Ku, S.Y. Lee, and S. Kim. 2011. Dual role of methionyl-tRNA synthetase in the regulation of translation and tumor suppressor activity of aminoacyl-tRNA synthetase-interacting multifunctional protein-3. *Proc. Natl. Acad. Sci. USA.* 108:19635–19640. http://dx.doi.org/10.1073/pnas.1103922108

Lacy, P., and J.L. Stow. 2011. Cytokine release from innate immune cells: association with diverse membrane trafficking pathways. *Blood.* 118:9–18. http://dx.doi.org/10.1182/blood-2010-08-265892

Man, S.M., and T.D. Kanneganti. 2016. Converging roles of caspases in inflammasome activation, cell death and innate immunity. *Nat. Rev. Immunol.* 16:7–21. http://dx.doi.org/10.1038/nri.2015.7

Mañes, S., G. Fuentes, R.M. Peregil, A.M. Rojas, and R.A. Lacalle. 2010. An isoform-specific PDZ-binding motif targets type I PIP5 kinase beta to the uropod and controls polarization of neutrophil-like HL60 cells. *FASEB J.* 24:3381–3392. http://dx.doi.org/10.1096/fj.09-153106

Mantovani, A., S. Sozzani, M. Locati, P. Allavena, and A. Sica. 2002. Macrophage polarization: tumor-associated macrophages as a paradigm for polarized M2 mononuclear phagocytes. *Trends Immunol.* 23:549–555. http://dx.doi.org/10.1016/S1471-4906(02)02302-5

Marzesco, A.M., P. Janich, M. Wilsch-Bräuninger, V. Dubreuil, K. Langenfeld, D. Corbeil, and W.B. Huttner. 2005. Release of extracellular membrane particles carrying the stem cell marker prominin-1 (CD133) from neural progenitors and other epithelial cells. *J. Cell Sci.* 118:2849–2858. http://dx.doi.org/10.1242/jcs.02439

Matsuo, H., J. Chevallier, N. Mayran, I. Le Blanc, C. Ferguson, J. Fauré, N.S. Blanc, S. Matile, J. Dubochet, R. Sadoul, et al. 2004. Role of LBPA and Alix in multivesicular liposome formation and endosome organization. *Science.* 303:531–534. http://dx.doi.org/10.1126/science.1092425

Meerschaert, K., E. Remue, A. De Ganck, A. Staes, C. Boucherie, K. Gevaert, J. Vandekerckhove, L. Kleiman, and J. Gettemans. 2008. The tandem PDZ protein Syntenin interacts with the aminoacyl tRNA synthetase complex in a lysyl-tRNA synthetase-dependent manner. *J. Proteome Res.* 7:4962–4973. http://dx.doi.org/10.1021/pr800325u

Mirando, A.C., C.S. Francklyn, and K.M. Lounsbury. 2014. Regulation of angiogenesis by aminoacyl-tRNA synthetases. *Int. J. Mol. Sci.* 15:23725–23748. http://dx.doi.org/10.3390/ijms151223725

Nechushtan, H., S. Kim, G. Kay, and E. Razin. 2009. Chapter 1: The physiological role of lysyl tRNA synthetase in the immune system. *Adv. Immunol.* 103:1–27. http://dx.doi.org/10.1016/S0065-2776(09)03001-6

Odorizzi, G. 2006. The multiple personalities of Alix. *J. Cell Sci.* 119:3025–3032. http://dx.doi.org/10.1242/jcs.03072

Ofir-Birin, Y., P. Fang, S.P. Bennett, H.M. Zhang, J. Wang, I. Rachmin, R. Shapiro, J. Song, A. Dagan, J. Pozo, et al. 2013. Structural switch of lysyl-tRNA synthetase between translation and transcription. *Mol. Cell.* 49:30–42. http://dx.doi.org/10.1016/j.molcel.2012.10.010

Ostrowski, M., N.B. Carmo, S. Krumeich, I. Fanget, G. Raposo, A. Savina, C.F. Moita, K. Schauer, A.N. Hume, R.P. Freitas, et al. 2010. Rab27a and Rab27b control different steps of the exosome secretion pathway. *Nat. Cell Biol.* 12:19–30.

Park, B.J., J.W. Kang, S.W. Lee, S.J. Choi, Y.K. Shin, Y.H. Ahn, Y.H. Choi, D. Choi, K.S. Lee, and S. Kim. 2005a. The haploinsufficient tumor suppressor p18 upregulates p53 via interactions with ATM/ATR. *Cell.* 120:209–221. http://dx.doi.org/10.1016/j.cell.2004.11.054

Park, M.C., T. Kang, D. Jin, J.M. Han, S.B. Kim, Y.J. Park, K. Cho, Y.W. Park, M. Guo, W. He, et al. 2012. Secreted human glycyl-tRNA synthetase implicated in defense against ERK-activated tumorigenesis. *Proc. Natl. Acad. Sci. USA.* 109:E640–E647. http://dx.doi.org/10.1073/pnas.1200194109

Park, S.G., H.J. Kim, Y.H. Min, E.C. Choi, Y.K. Shin, B.J. Park, S.W. Lee, and S. Kim. 2005b. Human lysyl-tRNA synthetase is secreted to trigger proinflammatory response. *Proc. Natl. Acad. Sci. USA.* 102:6356–6361. http://dx.doi.org/10.1073/pnas.0500226102

Park, S.G., H. Shin, Y.K. Shin, Y. Lee, E.C. Choi, B.J. Park, and S. Kim. 2005c. The novel cytokine p43 stimulates dermal fibroblast proliferation and wound repair. *Am. J. Pathol.* 166:387–398. http://dx.doi.org/10.1016/S0002-9440(10)62262-6

Piret, J.P., D. Mottet, M. Raes, and C. Michiels. 2002. $CoCl_2$, a chemical inducer of hypoxia-inducible factor-1, and hypoxia reduce apoptotic cell death in hepatoma cell line HepG2. *Ann. N. Y. Acad. Sci.* 973:443–447. http://dx.doi.org/10.1111/j.1749-6632.2002.tb04680.x

Potter, S.M., C.M. Wang, P.A. Garrity, and S.E. Fraser. 1996. Intravital imaging of green fluorescent protein using two-photon laser-scanning microscopy. *Gene.* 173:25–31. http://dx.doi.org/10.1016/0378-1119(95)00681-8

Quevillon, S., J.C. Robinson, E. Berthonneau, M. Siatecka, and M. Mirande. 1999. Macromolecular assemblage of aminoacyl-tRNA synthetases: identification of protein-protein interactions and characterization of a core protein. *J. Mol. Biol.* 285:183–195. http://dx.doi.org/10.1006/jmbi.1998.2316

Rosa, P., F.A. Barr, J.C. Stinchcombe, C. Binacchi, and W.B. Huttner. 1992. Brefeldin A inhibits the formation of constitutive secretory vesicles and immature secretory granules from the trans-Golgi network. *Eur. J. Cell Biol.* 59:265–274.

Ruiz-Ramos, R., L. Lopez-Carrillo, A.D. Rios-Perez, A. De Vizcaya-Ruíz, and M.E. Cebrian. 2009. Sodium arsenite induces ROS generation, DNA oxidative damage, HO-1 and c-Myc proteins, NF-κB activation and cell proliferation in human breast cancer MCF-7 cells. *Mutat. Res.* 674:109–115. http://dx.doi.org/10.1016/j.mrgentox.2008.09.021

Sampath, P., B. Mazumder, V. Seshadri, C.A. Gerber, L. Chavatte, M. Kinter, S.M. Ting, J.D. Dignam, S. Kim, D.M. Driscoll, and P.L. Fox. 2004. Noncanonical function of glutamyl-prolyl-tRNA synthetase: Gene-specific silencing of translation. *Cell.* 119:195–208. http://dx.doi.org/10.1016/j.cell.2004.09.030

Savina, A., C.M. Fader, M.T. Damiani, and M.I. Colombo. 2005. Rab11 promotes docking and fusion of multivesicular bodies in a calcium-dependent manner. *Traffic.* 6:131–143. http://dx.doi.org/10.1111/j.1600-0854.2004.00257.x

Son, S.H., M.C. Park, and S. Kim. 2014. Extracellular activities of aminoacyl-tRNA synthetases: New mediators for cell-cell communication. *Top. Curr. Chem.* 344:145–166. http://dx.doi.org/10.1007/128_2013_476

Sutton, E.J., T.D. Henning, B.J. Pichler, C. Bremer, and H.E. Daldrup-Link. 2008. Cell tracking with optical imaging. *Eur. Radiol.* 18:2021–2032. http://dx.doi.org/10.1007/s00330-008-0984-z

Théry, C., L. Zitvogel, and S. Amigorena. 2002. Exosomes: composition, biogenesis and function. *Nat. Rev. Immunol.* 2:569–579.

Théry, C., M. Ostrowski, and E. Segura. 2009. Membrane vesicles as conveyors of immune responses. *Nat. Rev. Immunol.* 9:581–593. http://dx.doi.org/10.1038/nri2567

Van Damme, P., L. Martens, J. Van Damme, K. Hugelier, A. Staes, J. Vandekerckhove, and K. Gevaert. 2005. Caspase-specific and nonspecific in vivo protein processing during Fas-induced apoptosis. *Nat. Methods.* 2:771–777. http://dx.doi.org/10.1038/nmeth792

Wieman, H.L., S.R. Horn, S.R. Jacobs, B.J. Altman, S. Kornbluth, and J.C. Rathmell. 2009. An essential role for the Glut1 PDZ-binding motif in growth factor regulation of Glut1 degradation and trafficking. *Biochem. J.* 418:345–367. http://dx.doi.org/10.1042/BJ20081422

Yannay-Cohen, N., I. Carmi-Levy, G. Kay, C.M. Yang, J.M. Han, D.M. Kemeny, S. Kim, H. Nechushtan, and E. Razin. 2009. LysRS serves as a key signaling molecule in the immune response by regulating gene expression. *Mol. Cell.* 34:603–611. http://dx.doi.org/10.1016/j.molcel.2009.05.019